Electronic Supplementary Information

Post–synthetic functionalization of Zn–CP by Tb^{3+} ions: ratiometric luminescent sensor for the ultraviolet filter benzophenone

Xu Zhang, Xin Li, Tianyang Ding, Jiahui Yu, Chengqi Jiao*, Ye Hu, Yanan Zhou, Yanyu Zhu*, Zhengang Sun* and Hanwen Zheng

School of Chemistry and Chemical Engineering, Liaoning Normal University, Dalian 116029, P. R. China

E-mail: jiaochengqi1989@163.com, summeryyzhu@163.com, szg188@163.com

CONTENTS:

Experimental Section

Materials and measurements

All reagents and solvents were purchased from commercial suppliers and utilized without further purification. The 4–carboxyphenylphosphonic acid (H_3pbc) was obtained as described in the literature.[1] Elemental analyses (C, H and N) were performed on a PE−2400 elemental analyzer. IR spectra were measured using a Bruker AXS TENSOR–27 FT–IR spectrometer from 4000 to 400 cm^{-1}. Thermogravimetric analyses (TG) were performed using a PerkinElmer Pyris Diamond TG–DTA thermal analyses system in the range of 50–1250 °C with a heating rate of 10 °C min^{-1}. Powder X–ray diffraction (PXRD) pattern was conducted on a Bruker AXS D8 ADVANCE diffractometer with Cu Kα radiation. UV–vis spectra were measured on a Lambda 35 spectrophotometer. Luminescent spectra were measured using a HITACHIF–7000 spectrofluorimeter. Luminescent lifetime was recorded on a HORIBA Scientifc FluoroMax–4 TCSPC spectrofluorometer. X–ray photoelectron spectra (XPS) were recorded on the Thermo SCIENTIFIC ESCALAB 250Xi photoelectron spectrometer. The highest occupied molecular orbital (HOMO) and the lowest unoccupied molecular orbital (LUMO) energy levels of H_3pbc ligand and BP were calculated by the DFT method at the B3LYP/6–31G*(d) level in the Gaussian 09 program package.[2] The triplet–state (T_1) level of H_3pbc ligand was calculated by the TD-DFT method at the B3LYP / 6–31G* (d) level in the Gaussian 09 program package.

X−ray crystallography

Data collections for **Zn–CP** were achieved on a Bruker AXS Smart APEX II CCD X–diffractometer with graphite–monochromated Mo Kα (λ = 0.71073 Å) at 296(2) K. The SHELX–2018 program was used to solve the structures by direct methods and refined on F^2 by full–matrix least–squares methods.[3] All non–H atoms were refined with anisotropic thermal parameters. The H atoms except those of water molecules were generated geometrically with fixed isotropic thermal parameters. A summary of the crystallographic data and refinement parameters are listed in Table S1. Bond distances and angles of **Zn–CP** are provided in Table S2.

Luminescent sensing experiments

Owing to BP is soluble in ethanol but insoluble in water, and the components in urine are soluble in water, the recognition system is carried out in mixed solvent (V_{EtOH} / V_{H2O} = 1: 1). Thus, as for the sensing experiments of common urine chemicals, 2.0 mg of **Zn–CP** or **Tb^{3+}@Zn–CP** powder was immersed into the mixed solvent (V_{EtOH} / V_{H2O} = 1: 1, 3.0 mL, 1.0 × 10^{-2} M), including different urine chemicals of KCl, NaCl, NH_4Cl, Na_2SO_4, urea, glucose (Glu), and BP, followed by ultrasonication for approximately 15 min, and then obtained the stable suspensions. Luminescent spectra of the suspensions were collected.

Luminescent titrations of BP

The luminescent spectra of the **Zn–CP** suspensions (2.0 mg **Zn–CP** in 3.0 mL deionized water after treating by ultrasonication for 15 min) were measured in situ after incremental addition of freshly prepared BP solutions (0–0.741 mM). After each addition, the luminescent spectrum of the suspension was monitored. **Zn–CP** shows a linear tendency in the quenching process, the luminescent quenching efficiency can be quantitatively explained by the linear Stern–Volmer (S–V) equation (1), and the limits of detection (LODs) were calculated by the equation (2):

$$I_0/I = 1 + K_{sv}[C] \quad (1) \qquad (1)$$

$$LOD = \frac{3\delta}{S} \qquad (2)$$

where K_{sv} is the quenching constant (M^{-1}), [C] is the molar concentration of quencher (BP), I_0 and I are the luminescent intensities before and after addition of BP, respectively. δ is the standard deviation and S is the slope of the obtained fitted line.

The luminescent spectra of the **Tb^{3+}@Zn–CP** suspensions (2.0 mg **Tb^{3+}@Zn–CP** in 3.0 mL deionized water after treating by ultrasonication for 15 min) were measured in situ after incremental addition of freshly prepared BP solutions (0–1.1 mM). After each addition, the luminescent spectrum of the suspension was monitored. **Tb^{3+}@Zn–CP** shows a linear tendency in the quenching process, the luminescent quenching efficiency can be quantitatively explained by the linear Stern–Volmer (S–V) equation (3), and the limits of detection (LODs) were calculated by the equation (4):

$$SD = \sqrt{\frac{1}{N-1}\sum_{I=1}(F - F_0)^2} \quad (3)$$

$$LOD = \frac{3SD}{|S|} \quad (4)$$

where *SD* is the standard deviation of replicate detection of blank solutions (N = 10), *F* is the relative luminescent intensities (I_L/I_{Tb}), F_0 is the average of *F* and *S* is the slope of the linear relationship in Fig. 6b.

Sensitivity experiments in real urine

For the sensitivity study of BP detection in real urine samples, the real urine system with different concentrations of BP was measured based on the above sensing methods. 1ml of human urine needs to be diluted 1000 times through the mixed solution to obtain the solution to be tested, [4, 5] and then 2.0 mg of **Zn–CP** or **Tb^{3+}@Zn–CP** powder was simply immersed into the 3.0 mL urine solutions treated by ultrasonication for approximately 15 min.

Recyclable luminescence experiments

The solid powder of **Zn–CP** after sensing BP was centrifuged for 10 minutes, then wash the solid powder three times with mixed solutions (V_{EtOH} / V_{H2O} = 1: 1), filter and dry, and then the sample is used for the next cycle experiment. The same operation is performed five times.

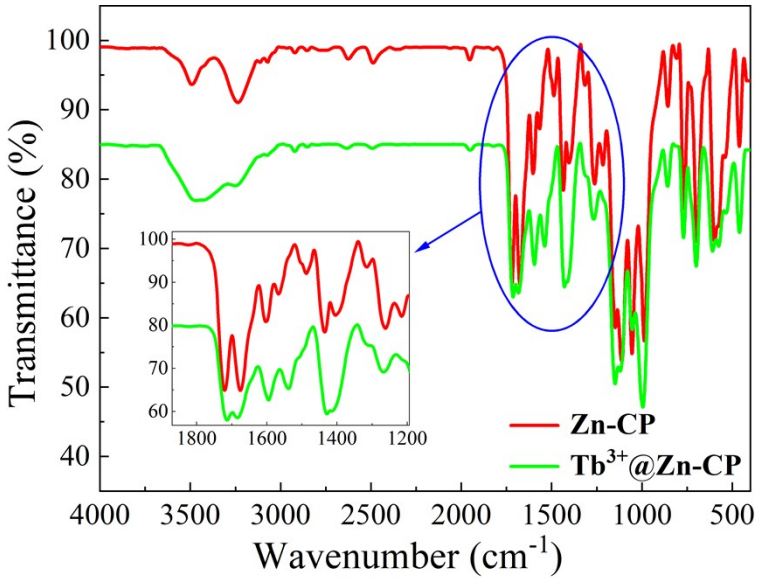

Fig. S1. IR spectra of **Zn–CP** and **Tb^{3+}@Zn–CP**.

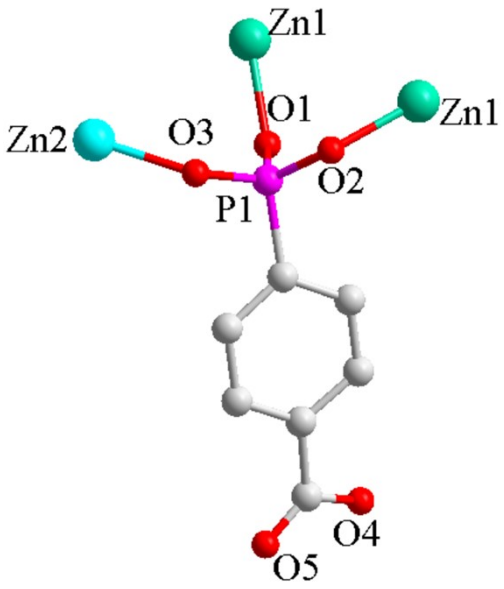

Fig. S2. Coordination mode of the $Hpbc^{2-}$ ligand in **Zn–CP**.

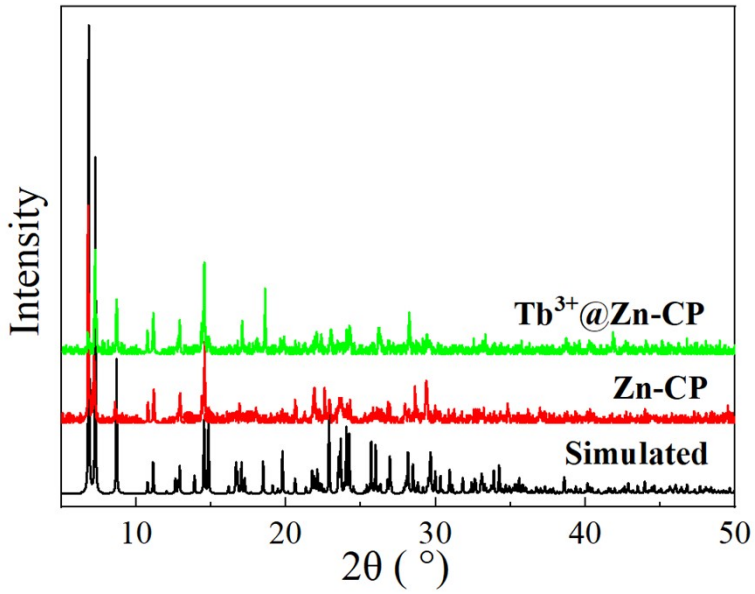

Fig. S3. PXRD spectra of **Zn–CP** and **Tb^{3+}@Zn–CP**.

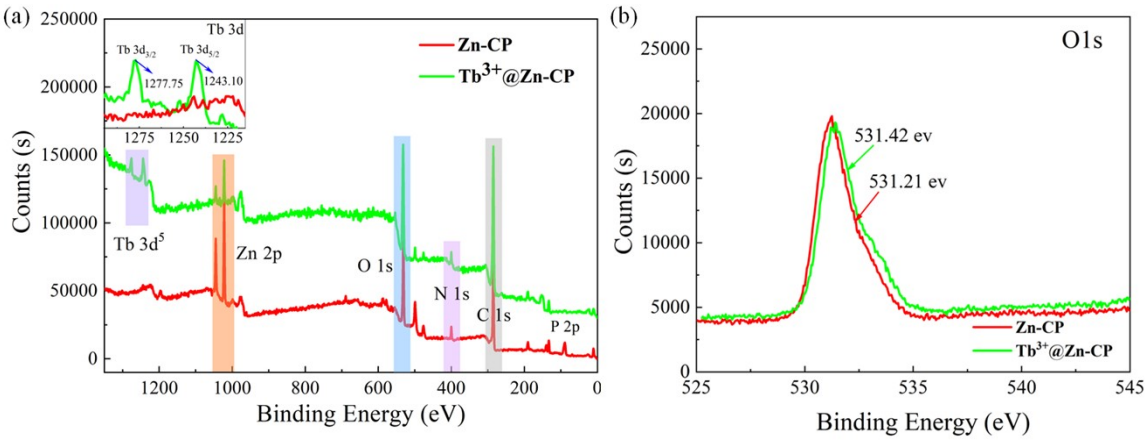

Fig. S4. (a) XPS full spectra of **Zn–CP** and **Tb^{3+}@Zn–CP**; (b) O1s XPS high-resolution spectra of **Zn–CP** and **Tb^{3+}@Zn–CP**.

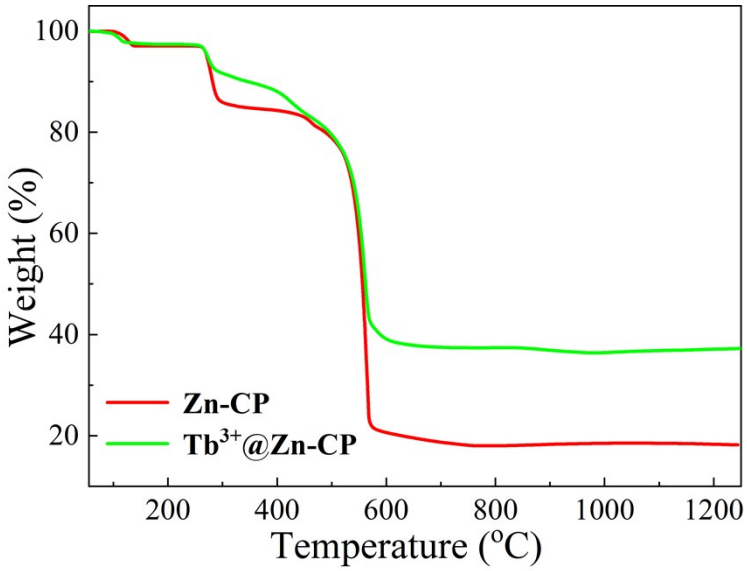

Fig. S5. TG curves of **Zn–CP** and **Tb^{3+}@Zn–CP**.

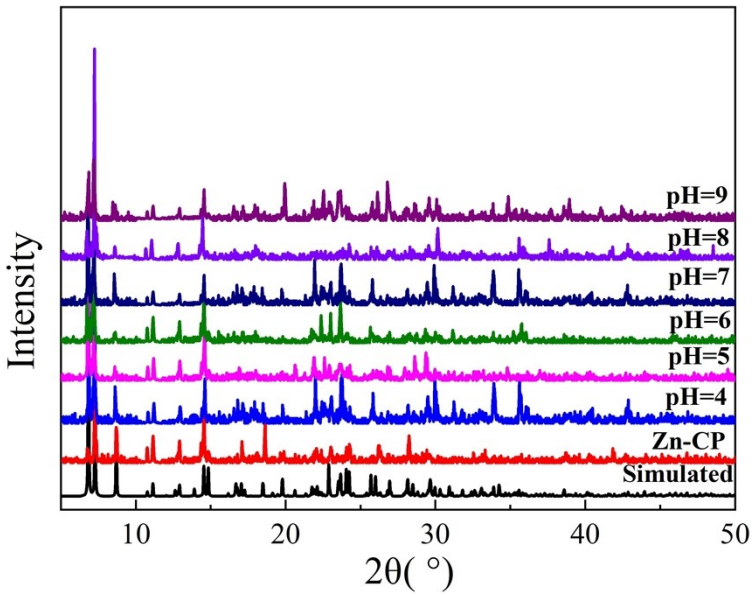

Fig. S6. PXRD spectra of **Zn–CP** immersed in mixed solutions (V_{EtOH} / V_{H2O} = 1: 1) with different pH for 24h.

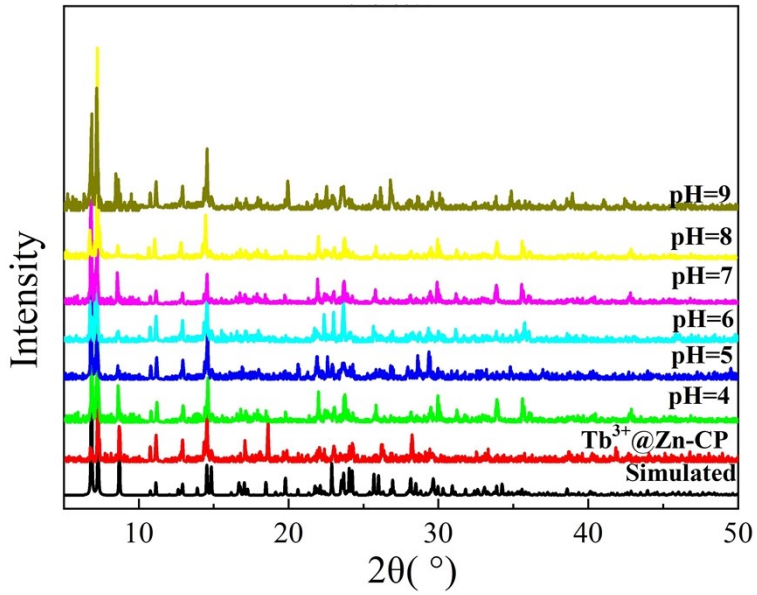

Fig. S7. PXRD spectra of **Tb^{3+}@Zn–CP** immersed in mixed solutions (V_{EtOH} / V_{H2O} = 1: 1) with different pH for 24h.

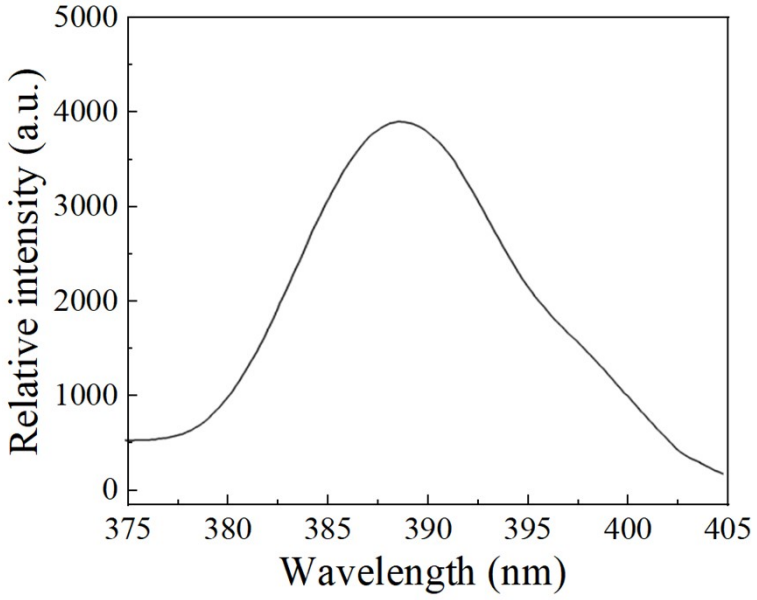

Fig. S8. Solid–state luminescent spectrum of 2, 2'–bipy.

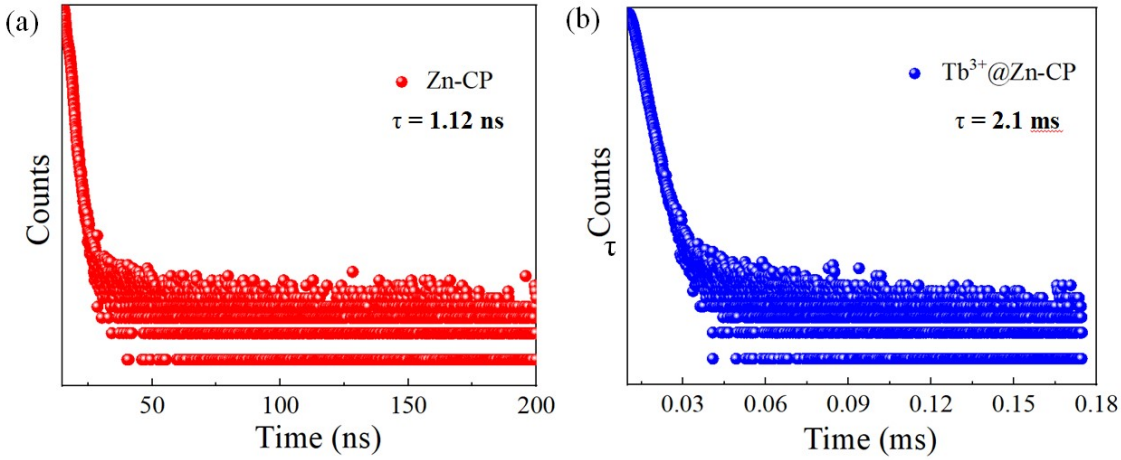

Fig. S9. Emission decay profiles of **Zn–CP** and **Tb^{3+}@Zn–CP**.

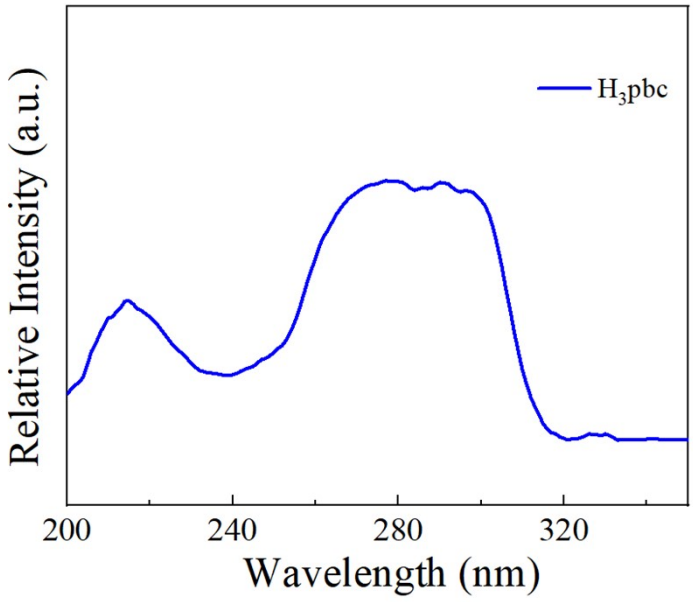

Fig. S10. UV–Vis absorption spectrum of H_3pbc.

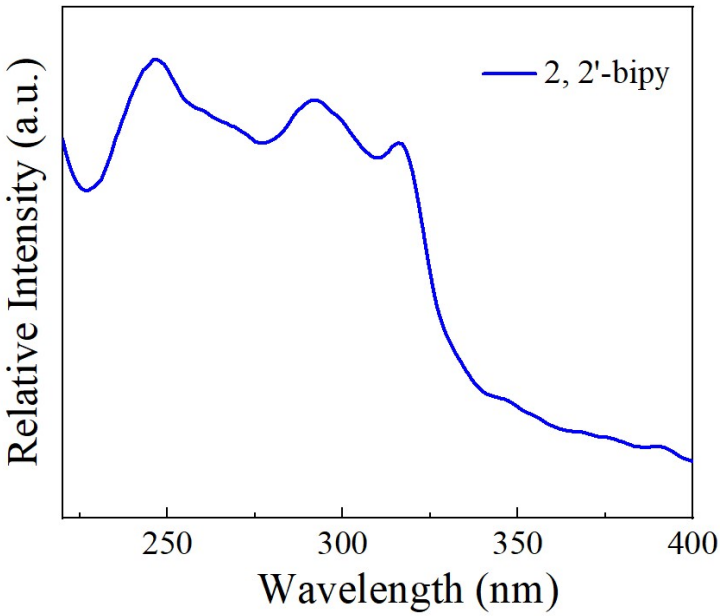

Fig. S11. UV–vis absorption spectrum of 2, 2'–bipy.

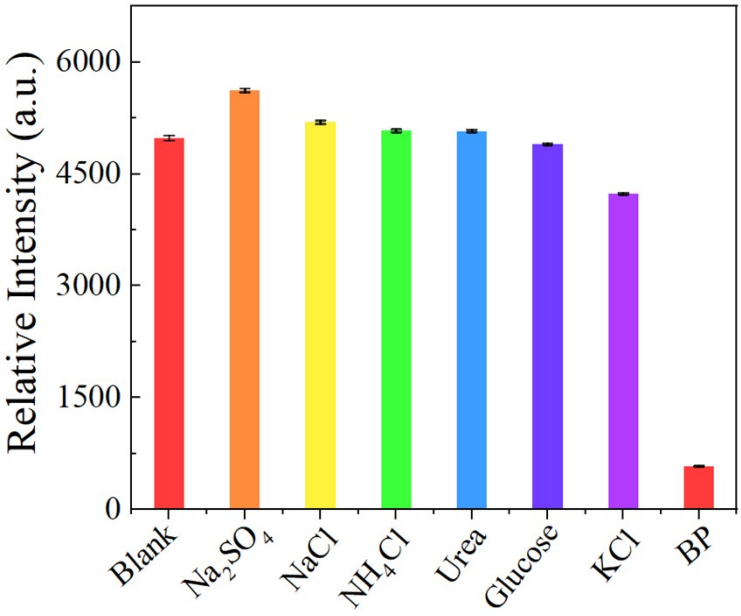

Fig. S12. Luminescent intensities of **Zn–CP** suspensions at 335 nm with various urine components.

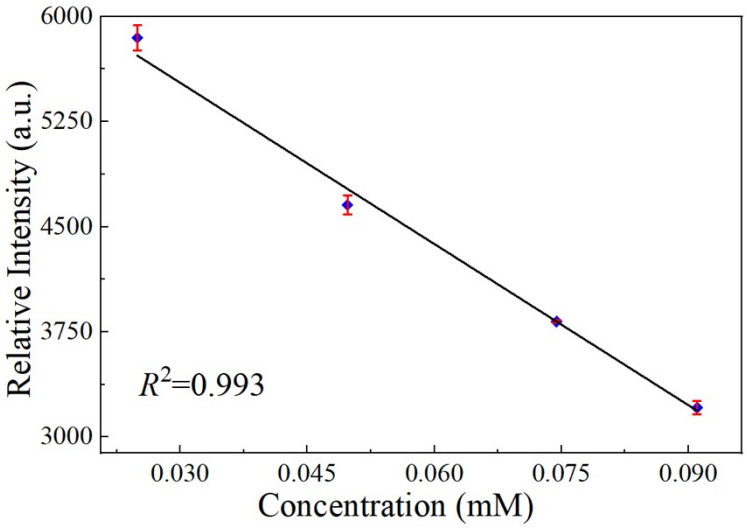

Fig. S13. The relationship between luminescent intensity of **Zn–CP** suspensions and the concentration of BP.

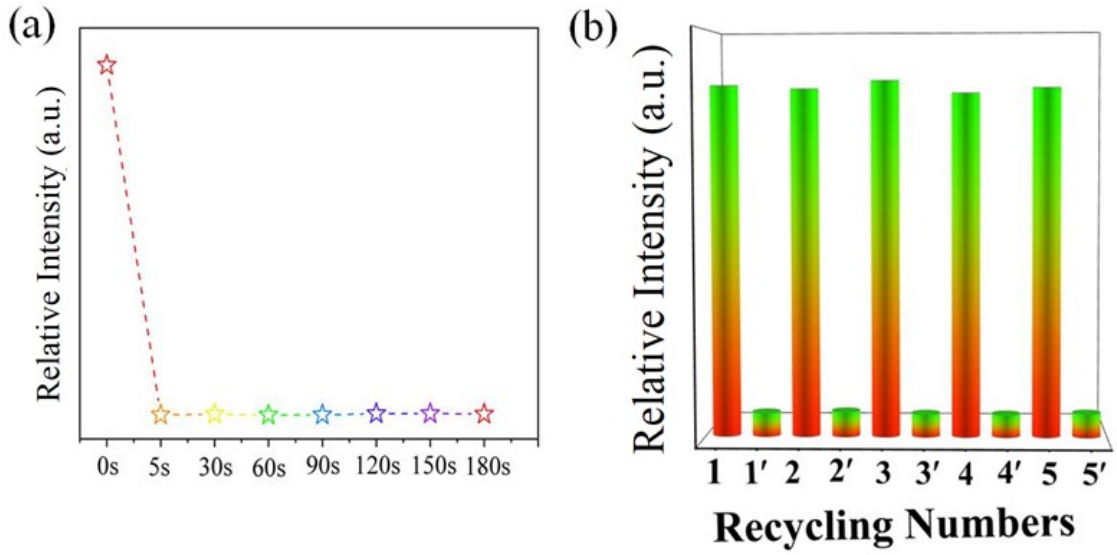

Fig. S14. (a) Emission spectra of **Zn–CP** suspensions after the addition of BP at different times; (b) Luminescent intensities of **Zn–CP** suspensions at 335 nm during five cyclic sensing experiments of BP in mixed solutions (V_{EtOH} / V_{H2O} = 1: 1).

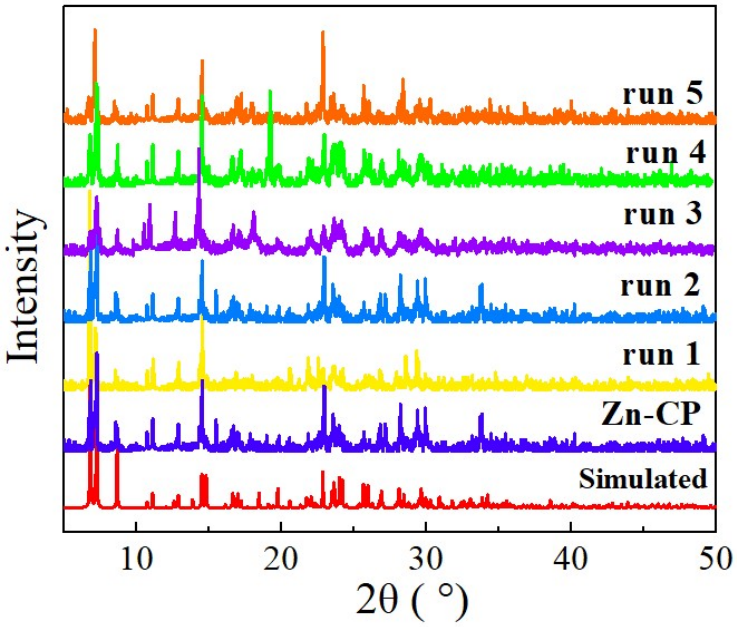

Fig. S15. PXRD patterns of **Zn-CP** after five recycles of sensing for BP in mixed solutions (V_{EtOH} / V_{H2O} = 1: 1).

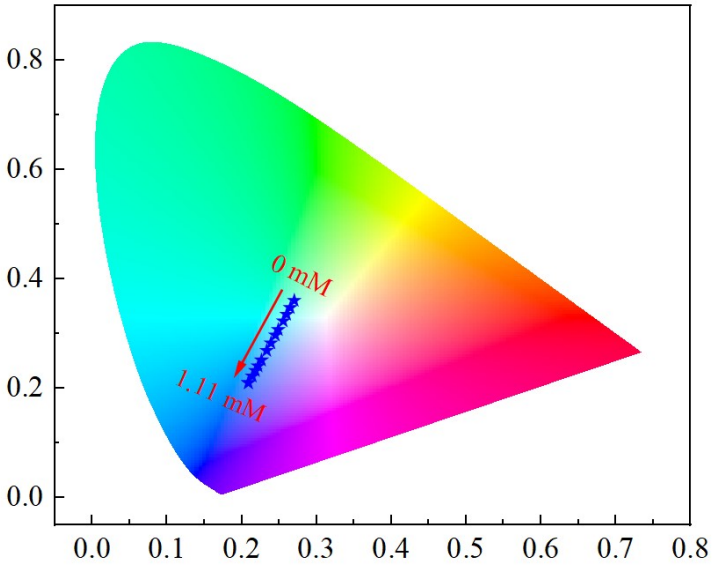

Fig. S16. CIE chromaticity diagram showing the variation of fluorescent color coordinates of the **Tb^{3+}@Zn–CP** dispersions in different BP concentrations (0–1.11 mM).

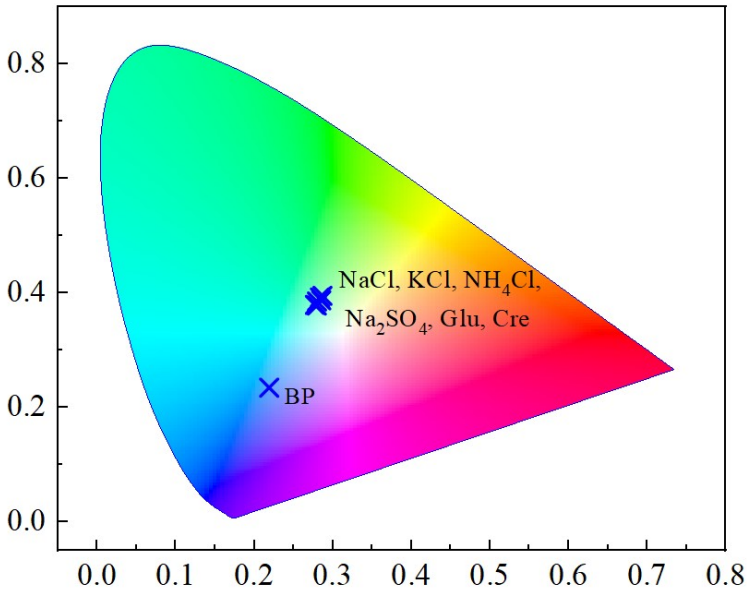

Fig. S17. CIE chromaticity diagram showing the variation of fluorescent color coordinates of the **Tb^{3+}@Zn–CP** dispersions in various urine components.

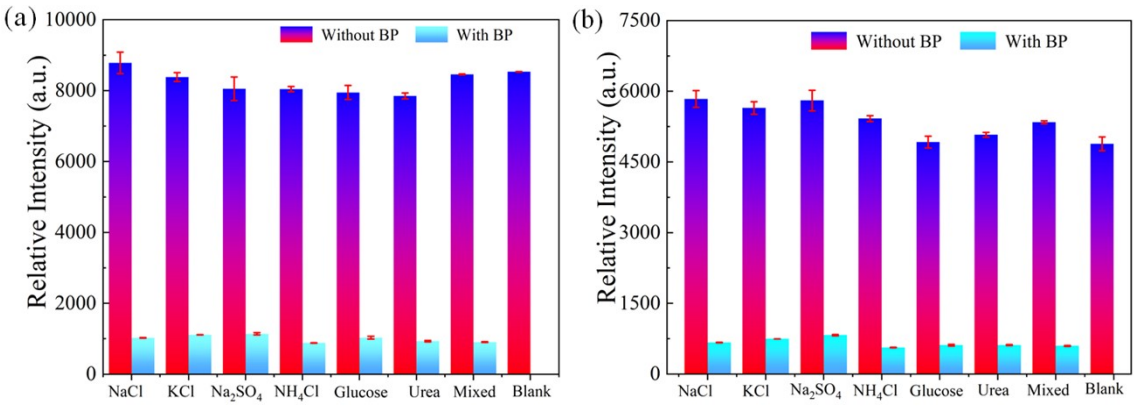

Fig. S18. Luminescent intensities of **Tb^{3+}@Zn–CP** suspensions at 343 nm (a) and 551 nm (b) included other individual or mixed substances in urine with and without the addition of BP.

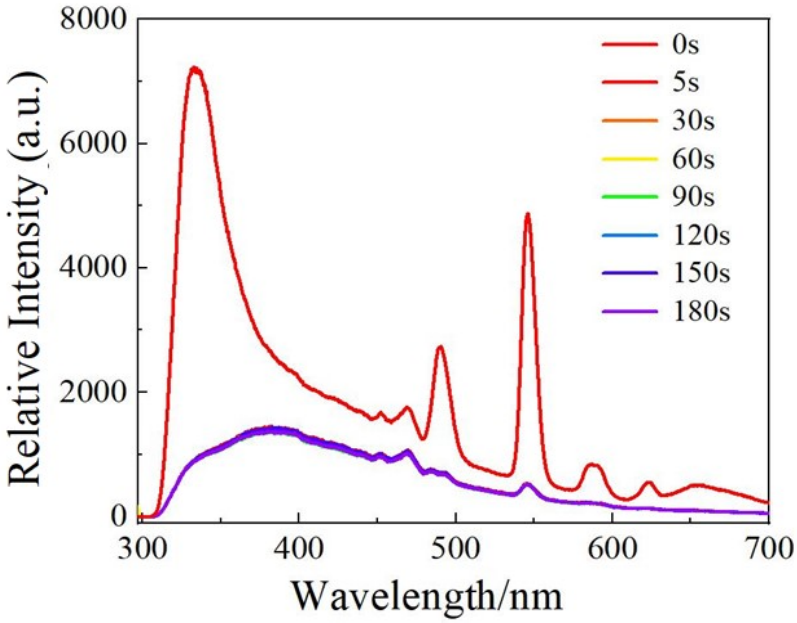

Fig. S19. Emission spectra of **Tb^{3+}@Zn–CP** suspensions after the addition of BP at different times

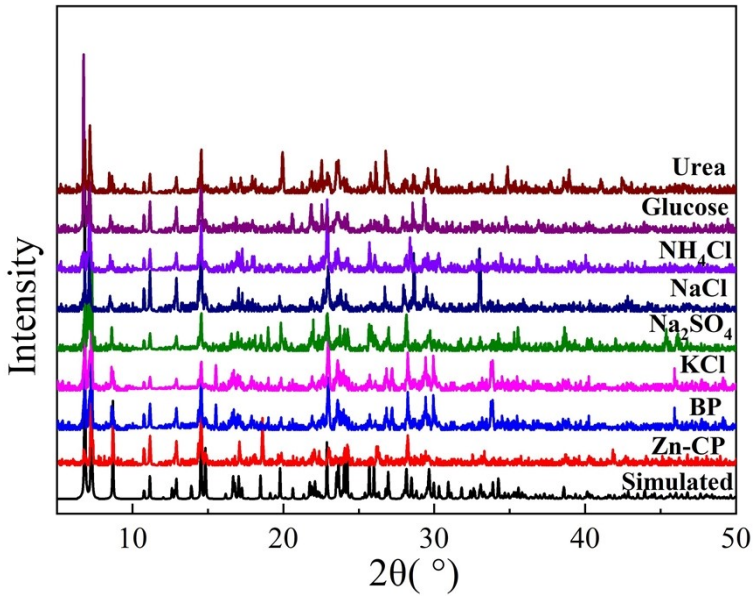

Fig. S20. PXRD patterns of **Zn–CP** immersing in mixed solutions (V_{EtOH} / V_{H2O} = 1: 1) with various urine chemicals.

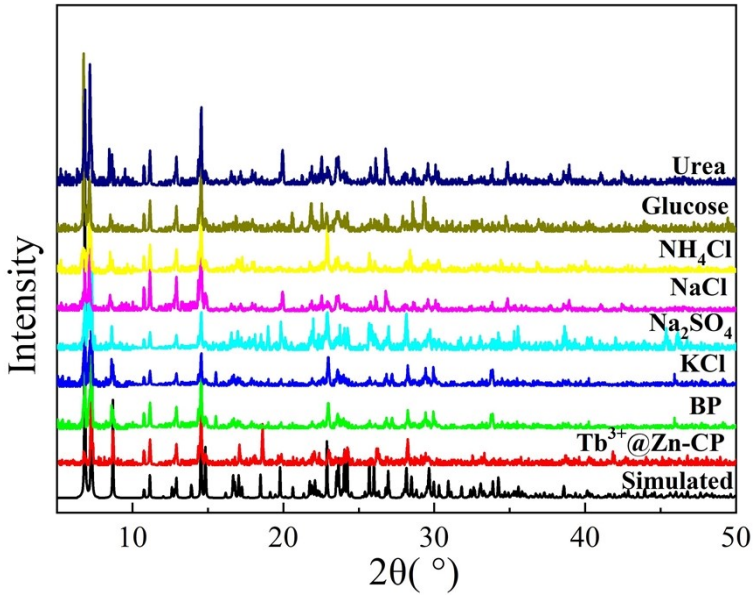

Fig. S21. PXRD patterns of **Tb^{3+}@Zn–CP** immersing in mixed solutions (V_{EtOH} / V_{H2O} = 1: 1) with various urine chemicals.

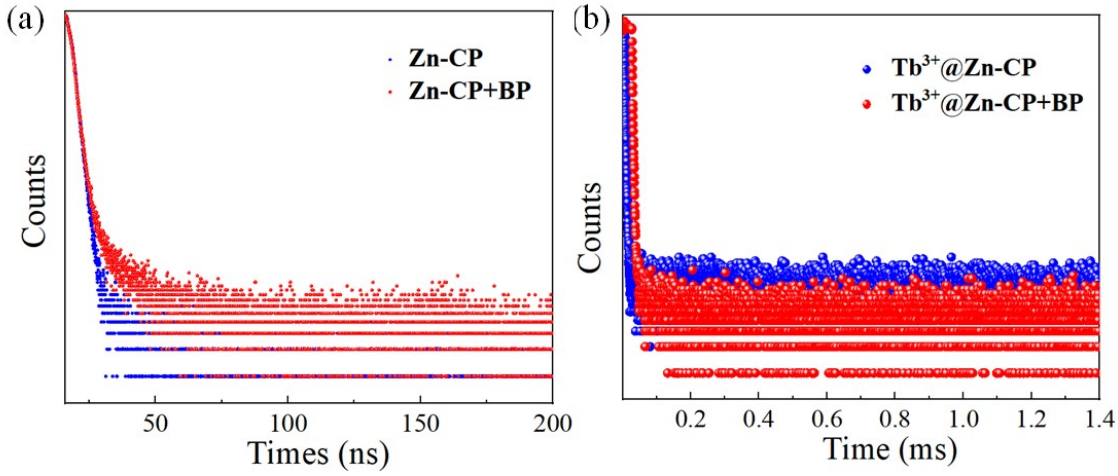

Fig. S22. Emission decay profiles of **Zn–CP** (a) and **Tb^{3+}@Zn–CP** suspensions (b) before and after sensing of BP.

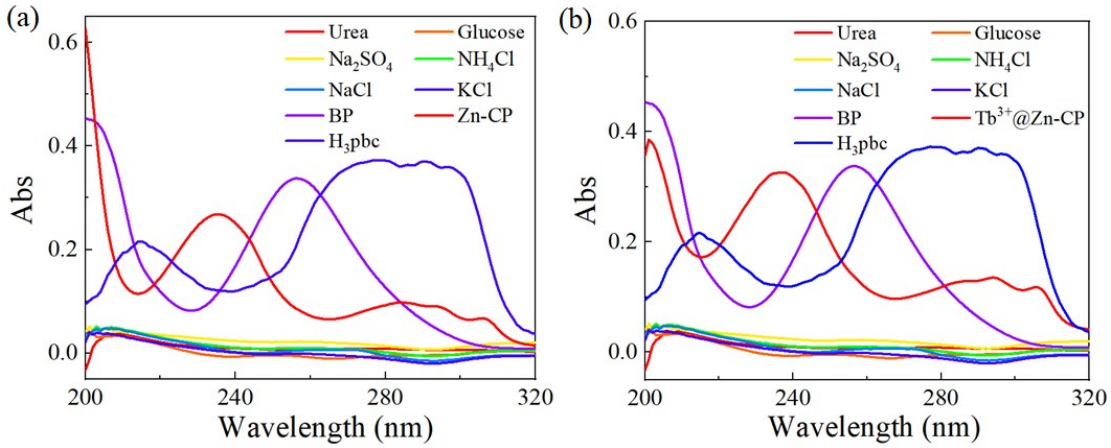

Fig. S23. UV–Vis absorption spectra of H_3pbc, **Zn–CP** (a) and **Tb^{3+}@Zn–CP** (b) towards various urine chemicals in mixed solutions (V_{EtOH} / V_{H2O} = 1: 1).

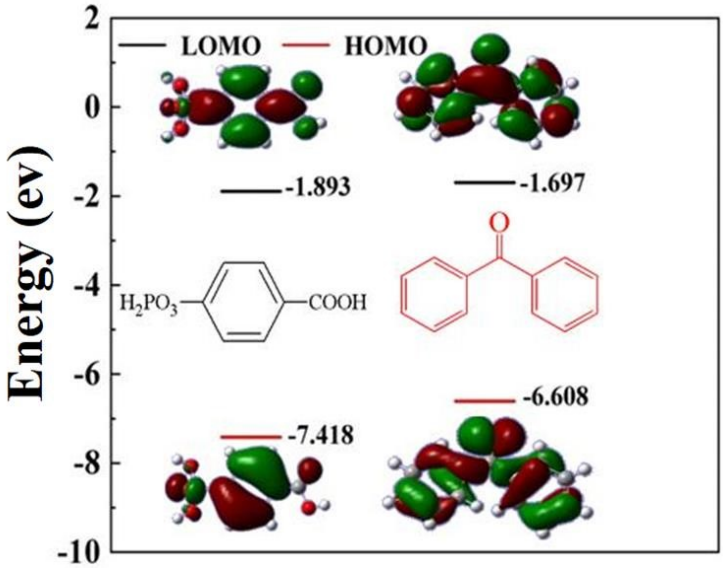

Fig. S24. HOMO and LUMO energy levels of the H_3pbc ligand and BP.

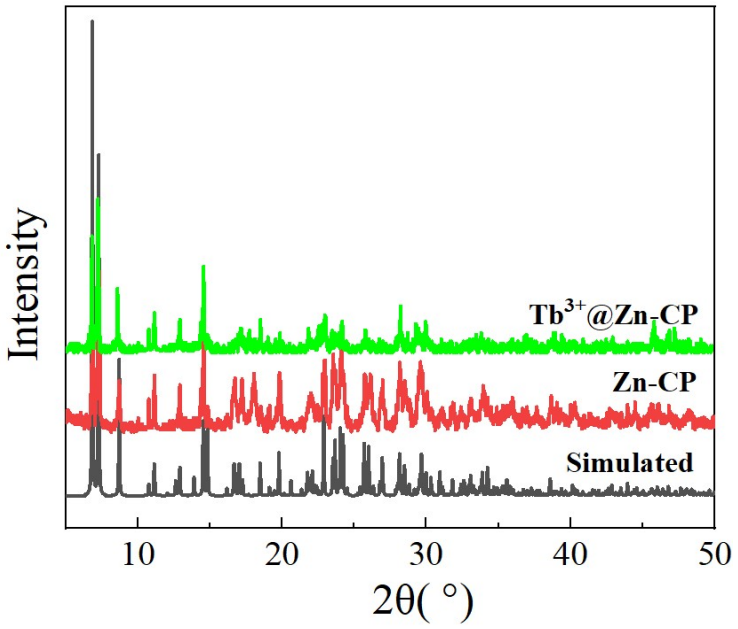

Fig. S25. PXRD patterns of **Zn–CP** and **Tb^{3+}@Zn–CP** immersing in real urine systems.

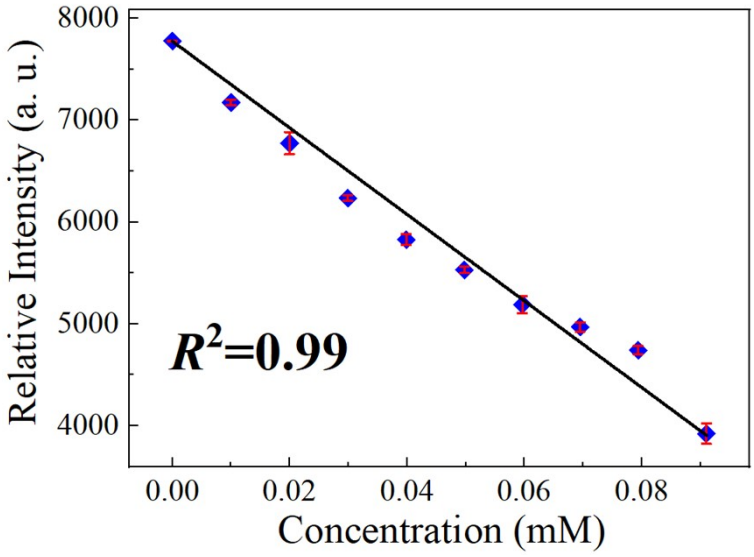

Fig. S26. The relationship between luminescent intensity of **Zn–CP** suspensions and the concentration of BP.

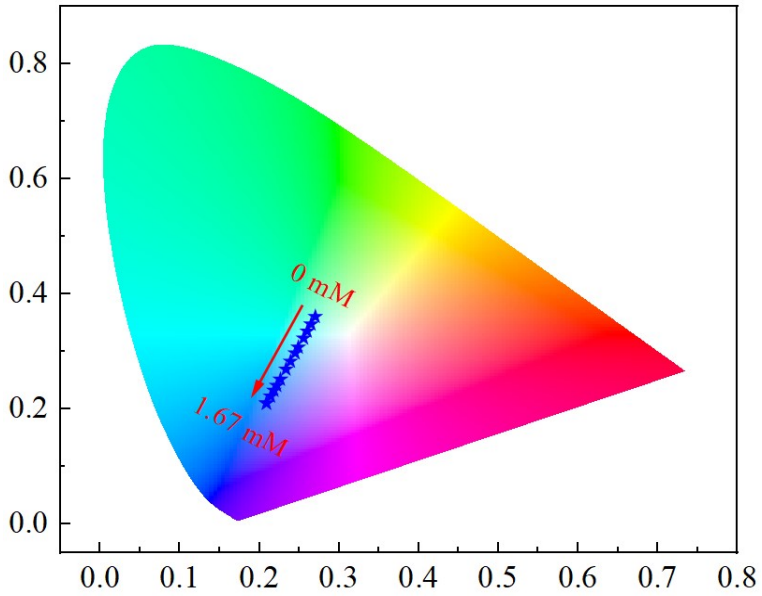

Fig. S27. CIE chromaticity diagram showing the variation of fluorescent color coordinates of the **Tb^{3+}@Zn–CP** dispersions in different BP concentrations (0–1.67 mM) in real urine systems.

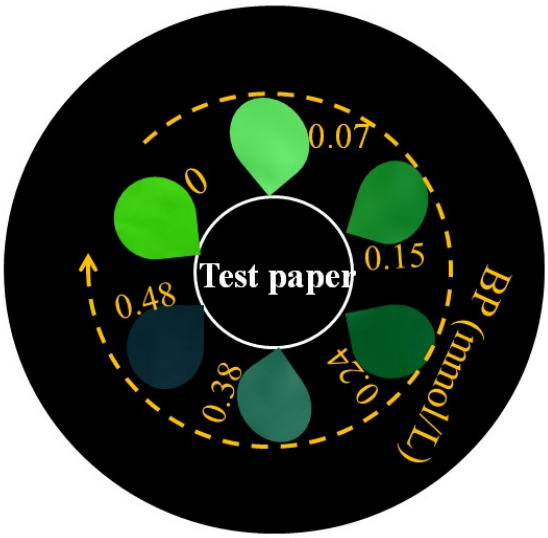

Fig. S28. Colors of the test papers of **Tb^{3+}@Zn–CP** upon the addition of BP with different concentrations in simulated urine systems.

Table S1. Crystal data and structure refinements for **Zn–CP**.

Compound	**Zn–CP**
Formular	$C_{24}H_{22}N_2O_{12}P_2Zn_2$
F*w*	723.11
Crystal system	Triclinic
Space group	$P\bar{1}$
a/Å	8.296
b/Å	12.679
c/Å	13.303
α/°	75.45
β/°	85.77
γ/°	80.51
V/Å^3	1335.25
Z	2
μ/mm^{-1}	1.799
Reflections collected	8320
Independent reflections	5971 [R_{int} = 0.0128]
Completeness to theta	99.5%
Goodness–of–fit on F^2	1.045
R_1, wR_2 [$I>2\sigma(I)$]	0.0273, 0.0650
R_1, wR_2 (all data)	0.0363, 0.0686

$R_1 = \Sigma (|F_0|-|F_C|) / \Sigma |F_0|$; $wR_2 = [\Sigma w (|F_0|-|F_C|)^2 / \Sigma w F_0^2]^{1/2}$.

Table S2. Selected bond lengths (Å) and angles (º) for **Zn–CP.**

Zn(1)–O(6)#1	1.9592(15)
Zn(1)–O(1)	1.9648(15)
Zn(1)–O(7)	2.1148(16)
Zn(1)–N(1)	2.125(2)
Zn(1)–N(2)	2.138(2)
Zn(2)–O(4)	1.9285(15)
Zn(2)–O(2)	1.9372(15)
Zn(2)–O(3)#2	1.9507(14)
Zn(2)–O(5)#3	1.9808(15)
P(1)–O(6)	1.5042(15)
P(1)–O(4)	1.5240(15)
P(1)–O(5)	1.5409(15)
P(2)–O(1)	1.5123(16)
P(2)–O(2)	1.5240(16)
P(2)–O(3)	1.5297(15)
O(6)#1–Zn(1)–O(1)	115.94(7)
O(6)#1–Zn(1)–O(7)	97.62(7)
O(1)–Zn(1)–O(7)	91.57(7)
O(6)#1–Zn(1)–N(1)	95.53(7)
O(1)–Zn(1)–N(1)	92.68(7)
O(7)–Zn(1)–N(1)	162.74(7)
O(6)#1–Zn(1)–N(2)	116.41(8)
O(1)–Zn(1)–N(2)	127.31(8)
O(7)–Zn(1)–N(2)	87.21(7)
N(1)–Zn(1)–N(2)	76.93(8)
O(4)–Zn(2)–O(2)	113.35(6)
O(4)–Zn(2)–O(3)#2	113.52(6)
O(3)#2–Zn(2)–O(5)#3	109.30(6)
O(4)–Zn(2)–O(5)#3	112.53(6)
O(2)–Zn(2)–O(5)#3	99.34(6)
O(2)–Zn(2)–O(3)#2	107.79(6)

Symmetry transformations used to generate equivalent atoms: #1 x+1, y, z ; #2 –x+1, –y+1, –z+2; #3 –x, –y+1, –z+2.

Table S3. ICP analyses for **Zn-CP** and **Tb^{3+}@Zn-CP.**

Samples	Amount of Zn^{2+} (%)	Amount of Tb^{3+} (%)
Zn-CP	8.95	0
Tb^{3+}@Zn-CP	7.58	5.12

Table S4. Comparison of the proposed sensor for BP detection with other methods.

Methods	Analyte	K_{sv} /M^{-1}	LOD	Refs.
LC–MS/MS	BP	–	2.35 ng L^{-1}	[S6]
MIP-GCE	BP	–	10 nM	[S7]
GC–MS	BP	–	0.5 ng L^{-1}	[S8]
GC–MS^n	BP	–	2 μg kg^{-1}	[S9]
HPLC–UV	BP	–	0.017 mg L^{-1}	[S10]
HPLC–UV	BP	–	0.046 mg L^{-1}	[S11]
Luminescent sensing	BP	6.67×10^3	1.81 μM	[S12]
Luminescent sensing	BP	1.57×10^4	4.67 μM	This work
Ratiometric luminescent sensing	BP	0.76×10^3	10.1μM	This work

Table S5. Luminescent lifetimes of **Zn–CP** and **Tb^{3+}@Zn–CP** suspensions before and after sensing of BP.

Materials	τ (ns)- λ_{em} = 322 nm / 343 nm	τ (ms)- λ_{em} = 551 nm
Zn–CP	0.409 ns	–
Zn–CP+BP	0.421 ns	–
Tb^{3+}@Zn–CP	0.379 ns	1.56 ms
Tb^{3+}@Zn–CP+BP	0.299 ns	1.51 ms

Reference

S1. I. P. Beletskaya, M. A. Kazankova, Catalytic Methods for Building up Phosphorus-Carbon Bond. *Russ. J. Org. Chem*. 2002, **38**, 1391−1430.

S2. M. J. Frisch, G. W. Trucks, H. B. Schlegel, G. E. Scuseria, M. A. Robb, J. R. Cheeseman, G. Scalmani, V. Barone, B. Mennucci, G. A. Petersson, H. Nakatsuji, M. Caricato, X. Li, H. P. Hratchian, A. F. Izmaylov, J. Bloino, G. Zheng, J. L. Sonnenberg, M. Hada, M. Ehara, K. Toyota, R. Fukuda, J. Hasegawa, M. Ishida, T. Nakajima, Y. Honda, O. Kitao, H. Nakai, T. Vreven, J. A. Jr. Montgomery, J. E. Peralta, F. Ogliaro, M. Bearpark, J. J. Heyd, E. Brothers, K. N. Kudin, V. N. Staroverov, R. Kobayashi, J. Normand, K. Raghavachari, A. Rendell, J. C. Burant, S. S. Iyengar, J. Tomasi, M. Cossi, N. Rega, J. M. Millam, M. Klene, J. E. Knox, J. B. Cross, V. Bakken, C. Adamo, J. Jaramillo, R. Gomperts, R. E. Stratmann, O. Yazyev, A. J. Austin, R. Cammi, C. Pomelli, J. W. Ochterski, R. L. Martin, K. Morokuma, V. G. Zakrzewski, G. A. Voth, P. Salvador, J. J. Dannenberg, S. Dapprich, A. D. Daniels, O. Farkas, J. B. Foresman, J. V. Ortiz, J. Cioslowski, D. J. Fox, Gaussian 09, Revision A. 02.

S3. G. M. Sheldrick, SHELXT−Integrated space−group and crystal−structure determination, *Acta Crystallogr*. *A*., 2015, **71**, 3−8.

S4. J. L. Manzooria, M. Amjadia, J. Soleymanib, E. Tamizic, A. Rezamandd, A. Jouybane, Determination of deferiprone in urine and serum using a terbium–sensitized luminescence method, *Luminescence*., 2012, **27**, 268–273.

S5. Y. F. Jiang, L. Li, X. Y. Sang, W. T. Chang, C. H. Zeng, C. H. Song, S. R. Sheng, Portable and luminescent fiber based sensing device for antibiotics in human urine and real water samples, *Dyes. Pigm.*, 2023, **209**, 110904.

S6. M. Krause, H. Frederiksen, K. Sundberg, F. S. Jørgensen, L. N. Jensen, P. Nørgaard, C. Jørgensen, P. Ertberg, A. Juul, K. T. Drzewiecki, N. E. Skakkebaek, A. M. Andersson, Presence of benzophenones commonly used as UV filters and absorbers in paired maternal and fetal samples, *Environ. Int*., 2018, **110**, 51−60.

S7. H. D. Li, H. M. Guan, H. Dai, Y. J. Tong, X. N. Zhao, W. J. Qi, S. Majeed, G. B. Xu, An amperometric sensor for the determination of benzophenone in food packaging materials based on

the electropolymerized molecularly imprinted poly-o-phenylenediamine film, *Talanta*., 99 2012, **99**, 811–815.

S8. M. Kawaguchi, R. Ito, H. Honda, N. Endo, N. Okanouchi, K. Saito, Y. Seto, H. Nakazawa, Simultaneous analysis of benzophenone sunscreen compounds in water sample by stir bar sorptive extraction with in situ derivatization and thermal desorption–gas chromatography–mass spectrometry, *J. Chromatogr. A*., 2008, **1200**, 260–263.

S9. E. Van Hoeck, T. De Schaetzen, C. Pacquet, F. Bolle, L. Boxus, J. Van Loco, Analysis of benzophenone and 4-methylbenzophenone in breakfast cereals using ultrasonic extraction in combination with gas chromatography–tandem mass spectrometry (GC–MSn), *Anal. Chim. Acta.*, 2010, **663**, 55–59.

S10. S. Pastorelli, A. Sanches-Silva, J. M. Cruz, C. Simoneau, P. P. Losada, Development of a Multimethod for the Determination of Photoinitiators in Beverage Packaging, *Eur. Food. Res. Technol*., 2008, **227**, 1585–1590.

S11. R. Koivikko, S. Pastorelli, A. R. B. de Quiros, R. Paseiro-Cerrato, P. Paseiro Losada, C. Simoneau, Rapid multi-analyte quantification of benzophenone, 4-methylbenzophenone and related derivatives from paperboard food packaging, *Food. Addit. Contam. A*., 2010, **27**, 1478–1486.

S12. Q. T. Xu, Z. H. Chen, H. Min, F. Song, Y. X. Wang, W. Shi, P. Cheng, Water Stable Heterometallic Zn–Tb Coordination Polymer for Rapid Detection of the Ultraviolet Filter Benzophenone, *Inorg. Chem*., 2020, **59**, 6729–6735.